Dynamics of Large Scale Motions in Bubble-Driven Turbulent Flow

Kyung Chun Kim

School of Mechanical Engineering,
Pusan National University
Jangjeon-dong, Geumjeong-gu, Pusan, 609-735, Korea
kckim@pusan.ac.kr

Seung Jae Yi, Sang Moon Kim, Hyun Dong Kim, Jong Wook Kim

Department of Mechanical Engineering,
Pusan National University
Jangjeon-dong, Geumjeong-gu, Pusan, 609-735, Korea

ABSTRACT

In this paper, the recirculation flow motion and mixing characteristics driven by air bubble flow in a rectangular water tank is studied. The Time-resolved PIV technique is adopted for the quantitative visualization and analysis. 532 nm Diode CW laser is used for illumination and orange fluorescent particle images are acquired by a PCO 10bit high-speed camera. To obtain clean particle images, 545 nm long pass optical filter and an image intensifier are employed and the flow rates of compressed air is changed from 2ℓ/min to 4ℓ/min at 0.5MPa. The recirculation and mixing flow field is further investigated by the POD analysis technique. It is observed that the large scale counterclockwise rotation and main vortex is generated in the upper half depth from the free surface and one quarter width from the sidewall. When the flow rates are increased, the main vortex core is moved to the side and bottom wall direction.

Fig 1. Experimental apparatus for bubbling mixer.

1. INTRODUCTION

Knowledge of bubbly flows is significant to various engineering systems such as nuclear waste treatment, bio-chemical reactors and steel making plant. Especially in the chemical engineering and industrial field, the mixing problems such as powder dispersion, solid blending, and gas dispersion into liquid have been an important issue because product quality and productivity highly depend on the mixing process[1, 2, 3]. To enhance mixing efficiency or for high temperature mixing condition, air bubbling can be used. In addition the great interest in the multiphase flow is the interaction of the dispersed phase with the underlying turbulent flow. In this study, the entire flow structure and flow characteristic with varying flow rates within a rectangular tank are identified by using PIV and POD techniques for the bubbling mixer.

2. EXPERIMENTAL SETUP

In this study, a typical 2-dimensional time-resolved PIV system is adopted as shown in Fig.1. A PCO 10bit high speed CCD camera (1K × 1K) is used for orange fluorescent particle(D_p=10µm, λ_{ex}=540nm, λ_{em}=584nm) imaging and a laser sheet beam of 2mm thickness created by a spherical lens and cylindrical lens was irradiated to the object plane from Ar-ion CW laser for illumination. The field-of-view size is 100 mm × 90 mm and measurement (laser sheet) position is the center of bubbler. Final vector fields were acquired through the interrogation by the PIV-Sleuth program. Tab water was used as a working fluid and compressed air is used for formation of bubble stream. Air flow rate was 3 l /min at 0.5MPa.

3. PROPER ORTHOGONAL DECOMPOSITION

Dynamic information of the flow field can be explained effectively by POD (Proper Orthogonal Decomposition), from which the relative energy distribution is acquired. By using the POD technique as proposed by Lumley, The flow field can be decomposed into optimal orthogonal spatial modes and optimal orthogonal temporal modes.

$$\mathbf{u}(\mathbf{x},t) = \sum_n a^{(n)}(t)\boldsymbol{\varphi}^{(n)}(\mathbf{x})$$

(1)

The optimality means that POD minimizes the mean square error of any partial sum of expansion and conversely the expansion in terms of these bases obtained by POD converges faster than the expansion in terms of any other basis such as Fourier decomposition. The spatial modes $\varphi^{(n)}(\mathbf{x})$ can be obtained by solving the following integral equation:

$$\int R(\mathbf{x},\mathbf{x}')\varphi^{(n)}(\mathbf{x}')d\mathbf{x} = \lambda^{(n)}\varphi^{(n)}(\mathbf{x}) \tag{2}$$

where λ is the eigenvalue, and $R(\mathbf{x},\mathbf{x}')$ is ensemble-averaged two point correlation function, $\langle \mathbf{u}(\mathbf{x})\mathbf{u}(\mathbf{x}')\rangle$. The orthogonality of spatial basis and temporal basis is represented as followings as

$$\left(\varphi^{(n)}(\mathbf{x}),\varphi^{(m)}(\mathbf{x}')\right) = \delta_{nm} \ , \ \left\langle a^{(n)}(t),a^{(m)}(t)\right\rangle = \lambda^{(n)}\delta_{nm} \tag{3}$$

The traditional direct method requires huge calculations, so it takes much time, but Sirovich[5] suggested the method of snapshot that can save calculation time. In this research, in order to find the dynamic structures, we executed a POD analysis using the method of snapshots and the instantaneous fluctuating velocity field:

$$\mathbf{u}(\mathbf{x},t) = \overline{\mathbf{u}}(\mathbf{x}) + \mathbf{u}'(\mathbf{x},t) = \overline{\mathbf{u}}(\mathbf{x}) + \sum_{m=1}^{M} a^{(m)}(t)\varphi^{(m)}(\mathbf{x}) \tag{4}$$

From the calculated eigenmodes, we extracted the turbulent kinetic energy contribution, and compared it with a large-scale structure using the sum of first few modes.

4. RESULTS AND DISCUSSIONS

Fig.2 represents the time-mean velocity field driven by single bubble stream for each case. It can be seen that there is upstream driven by the bubble stream at the right side of plot and the counter-clockwise large vertical structure is located at the upper left side. We can observe the inflow of fluid at the left-bottom side of view, because of the rising air bubble at the right side. Compare mean velocity field with each case (a), (b) and (c), we can observe the movement of center of vertical structure. In the case of (a), the structure core location is $X/D_N=3.7$, $Y/D_N=9.0$, but in the case of (c), the location of structure core is $X/D_N=2.7$, $Y/D_N=7.7$. In this way, we can know that as flow rates are increased, the center of structure is moved to left-bottom side, and it is because of the increase of upstream energy. While the flow rate is increased, the upstream energy is also increased.

In POD analysis of this study, the eigenvalue represent the turbulent kinetic energy of each mode. Fig. 3 demonstrates the turbulent kinetic energy distribution and the corresponding cumulative energy sum with respect to the mode number for each case. The time-mean flow average field has about 75% of total kinetic energy at the case (a), which is the dominant dynamic structure in the set of instantaneous velocity fields. It is shown that most of turbulent kinetic energy concentrate on the first few modes and the first 20 modes has about 82.4% of total turbulent kinetic energy (95.6% of total kinetic energy) at the case (a). The energy percentage of time-mean flow average field at the case (a) is 75% of total kinetic energy, but case (b) and case (c) is 71% and 62% energy distribution. While the flow rate is increased, the number of bubbles and vibration of

(a) Case Ⅰ (Q=2ℓ/min)   (b) Case Ⅱ (Q=3ℓ/min)   (c) Case Ⅲ(Q=4ℓ/min)
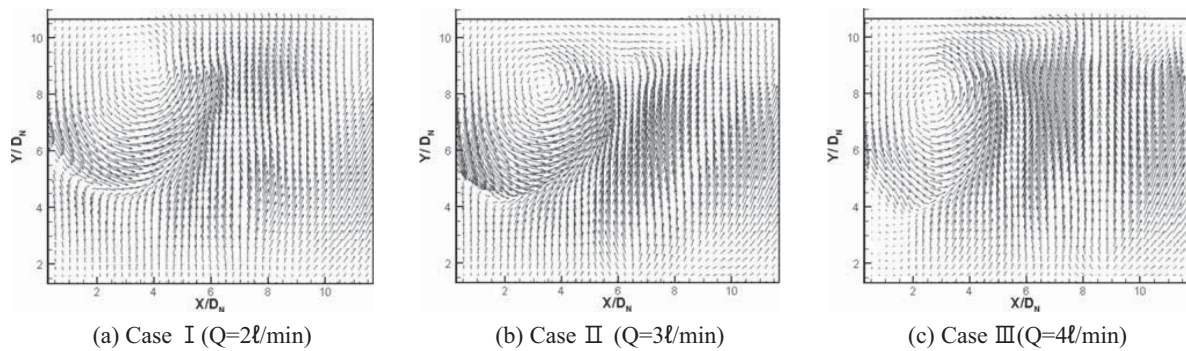
Fig 2. Mean velocity vector plot for each cases.

Energy percentage of average velocity field		
2ℓ/min	3ℓ/min	4ℓ/min
75%	71%	62%

(a) Cumulative percentage sum of energy   (b) Cumulative percentage sum of turbulent energy
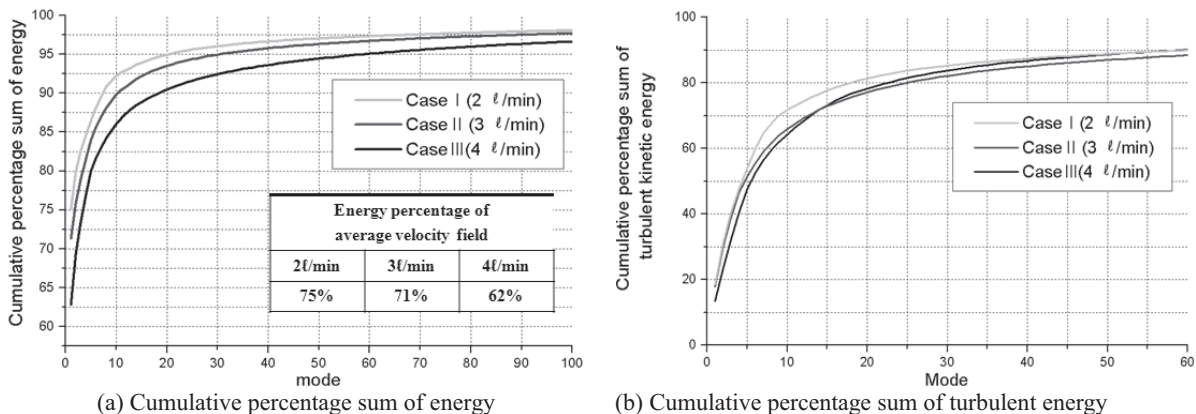
Fig 3. Energy distribution of sum of each mode.

Sixth International Symposium on Turbulence and Shear Flow Phenomena
Seoul, Korea, 22-24 June 2009
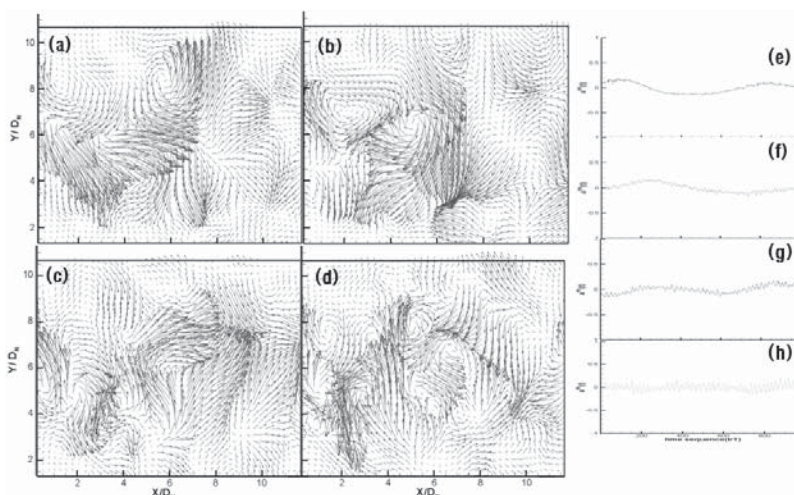
Fig 4. Velocity vector plots of eigen modes at Q=2ℓ/min; (a) 1st spatial mode, (b) 2nd spatial mode, (c) 3rd spatial mode, (d) 4th spatial mode, (e) 1st temporal mode, (f) 2nd temporal mode, (g) 3rd temporal mode, (h) 4th temporal mode
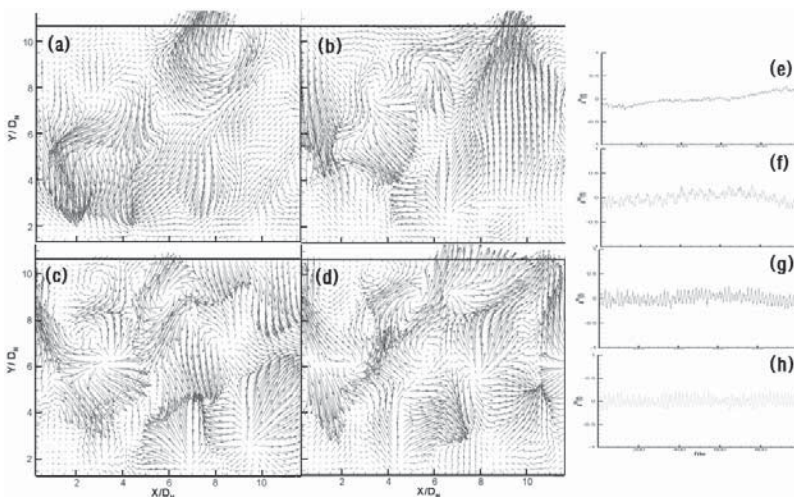
Fig 5. Velocity vector plots of eigen modes at Q=3ℓ/min; (a) 1st spatial mode, (b) 2nd spatial mode, (c) 3rd spatial mode, (d) 4th spatial mode, (e) 1st temporal mode, (f) 2nd temporal mode, (g) 3rd temporal mode, (h) 4th temporal mode
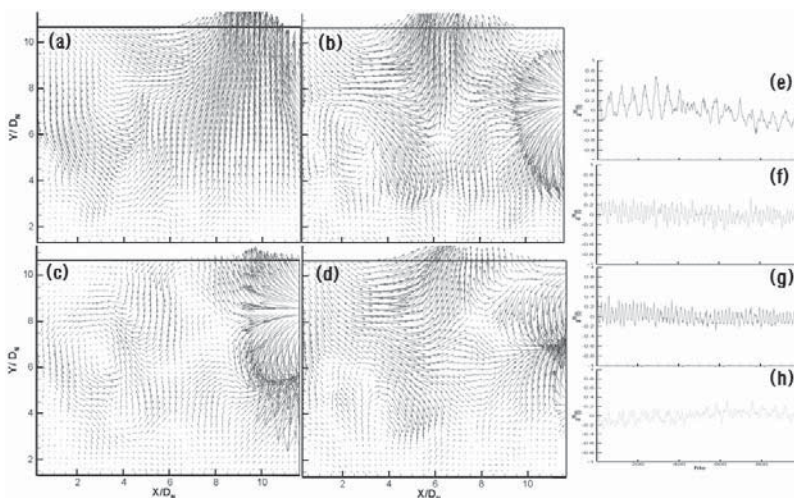
Fig 6. Velocity vector plots of eigen modes at Q=4ℓ/min; (a) 1st spatial mode, (b) 2nd spatial mode, (c) 3rd spatial mode, (d) 4th spatial mode, (e) 1st temporal mode, (f) 2nd temporal mode, (g) 3rd temporal mode, (h) 4th temporal mode
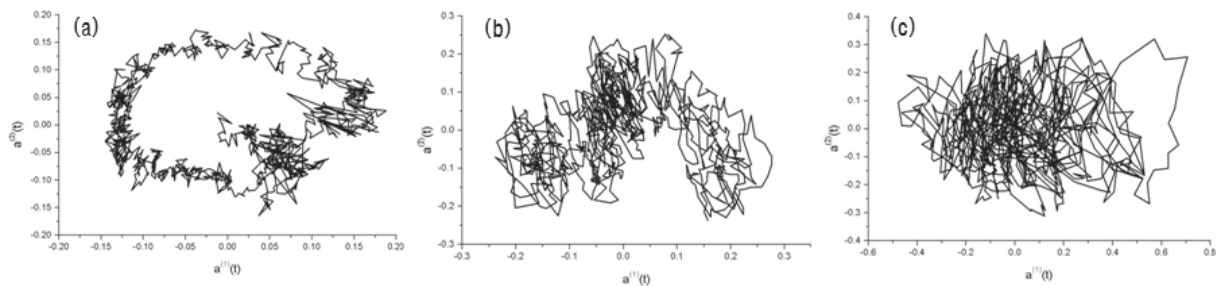
Fig 7. Phase space projection of 1st temporal mode and 2nd temporal mode; (a) Q=2ℓ/min, (b)Q=3ℓ/min, (c) Q=4ℓ/min

bubbles are also increased. It is mean that the term of turbulent kinetic is increased, so turbulent kinetic energy is changed because of the flow rate of air.

Figs 4 – 6 show the first 4 spatial and temporal modes which represent dynamics of large scale motions in turbulent mixing flow for three different flow rates respectably. Fig 4 demonstrates initial eigenmode at the flow rate is 2ℓ/min, the first mode (a) contains the largest turbulent energy. One can recognize rising flow due to bubbles at the right side and several small scale vertical motions are observed in the flow field. Those eddies are not seen in Fig 2, and randomly distributed in the flow field so that averaged field has a single large scale vortex in the measurement plane. Figs 4(c), (d) depict the third and forth eigenmodes which reveal the large scale structure become smaller and smaller through turbulent energy cascading. Higher modes appeared in Figs. (c) and (d) are not dominant in the overall flow field compared with (a) and (b), however those motions certainly contribute to turbulent mixing behavior. Fig 5 shows large scale eigenmodes in case of the flow rate is 3 ℓ/min. Compared with Fig. 4, it is observed that the scale of large scale vortex near free surface gets bigger and rising flow due to bubble can be recognized. With increasing flow rate of air, the rising velocity of bubbles is higher and associated vibrating motion generates turbulence more than that of the lower flow rate. The increased kinetic energy of bubble creates free surface vibration followed by higher rising velocity near the free surface and randomly distributed smaller vortices in higher eigenmodes as shown in Figs 5(c) and 5(d). Fig 6 shows the first four eigenmodes when the air flow rate is 4ℓ/min. Those are quite different compared with Fig 4 and Fig 5, and much more simple than lower flow rate cases. It can be explained that the energy cascading process begins at higher modes and energy spectrum of turbulent transport becomes wider due to increasing Reynolds number. All the spatial modes present rising flow near bubble and large scale vortex induced by free surface flow. Smaller scale motions are not shown in Figs 6 (c) and (d) since the energy containing eddies are dominated by the higher bubble rising velocity and free surface flow.

Corresponding temporal modes are depicted in Figs 5(e) to 5(h) when the flow rate is 2ℓ/min. Temporal modes present the variation of each spatial mode in time domain. As flow rate is increasing, the vibration of temporal mode increases. With increasing the air flow rate, the bubble generating time is decreasing and the rising velocity is increasing. As a result, the vibration of bubble itself is increased. In summary, at the lower flow rate, the geometrical complexity in spatial mode looks severe while temporal variation is rather simple. At higher flow rate, the complexity in the temporal mode becomes higher compared with spatial modes.

Fig. 7 represents the phase-space projection of the 1st temporal mode and the 2nd temporal mode for each case. It is shown that the projection has approximately circular shape with small oscillation along the circular shape at the case (a). The phase-space projection shows the periodic nature in small and large time scales. However, the phase-space projection of case (b) is similar with half circle, and the phase-space projection of case (c) is just like a dot. To analyze the correlation of two temporal modes in the last two cases, the appropriate frame rate adjustment is necessary.

5. CONCLUSION

To investigate the characteristics of the bubble-driven flow with varying flow rate, 300mm×300mm square tank, the nozzle is located at the bottom, is used and the flow rate is changed from 2 ℓ/min to 4 ℓ/min. The time-resolved PIV and POD technique is adopted for the quantitative visualization and analysis, and the measured flow field is investigated by POD technique. In this way, we get the following results.

All three cases occurs the anti-clockwise direction flow field because of the rising bubbles at the right side, and the main vortex is formed in the upper left. As the flow increases, the energy of rising bubble is larger, and the main vortex is moved to the side and bottom wall direction.

The time-mean flow average field at the case (a) has about 75% of total kinetic energy, and case (b) and case (c) is 71% and 62% energy distribution. While the flow rate is increased, the term of turbulent kinetic is also increased, so turbulent kinetic energy is changed because of the flow rate of air.

At the case (a), the phase-space projection of the 1st temporal mode and the 2nd temporal mode is shown that the projection has approximately circular shape with small oscillation along the circular shape, and case (b) and case (c) is similar with half circle and a dot. To analyze the correlation of two temporal modes in the last two cases, the appropriate frame rate adjustment is necessary.

REFERENCES

Luewisutthichat, W., Tsutsumi, A. and Yoshida, K., 1997, "Chaotic Hydrodynamics of Continuous Single-Bubble Flow Systems", *Chem. Eng. Sci.*, **52**, 3685-3691.

Tirto, P., Koichi, T. and Hideki, T., 2001, "Effect of Operating Conditions on Two-Phase Bubble Formation Behavior at Single Nozzle Submerged in Water", *J. Chem. Eng.* Japan, 34(2), 114-120.

Tu, X ; Trägårdh, C, 2002, "Methodology development for the analysis of velocity particle image velocimetry images of turbulent, bubbly gas-liquid flows", *Measurement science & technology*, 13(7), 1079-1086.

S. J. Yi, J. W. Kim, H. D. Kim, K. C. Kim, 2008, "Characteristics of Bubble-driven Flow by Using Time-resolved PIV and POD Technique", *The Korea Society of Visualization*, Vol. 6, No. 1, pp.41~46.

Montante. G, Horn. D., Paglianti. A., 2008, "Gas-liquid flow and bubble size distribution in stirred tanks", *Chemical engineering science*, Vol 63, No. 8, pp.2107-2118.

Kim, K. C., Min, Y. U., Oh, S. J., An, N. H., Seoudi, B., Chun, H. H., Lee, I., 2007, ″Time-Resolved PIV Investigation on the Unsteadiness of a Low Reynolds Number Confined Impinging Jet", *Journal of visualization*, Vol. 10, No.4 , pp.367-380.

Sirovich, L., 1987, "Turbulence and The Dynamics of Coherent Structures PART I : Coherent Structures", *Quarterly of Applied Mathematics*, Vol. 45, pp.561-571.